IEEE Access
Multidisciplinary | Rapid Review | Open Access Journal

Received December 1, 2017, accepted January 4, 2018, date of publication January 31, 2018,
date of current version February 28, 2018.

Digital Object Identifier 10.1109/ACCESS.2018.2796646

Contrast Enhancement of Microscopy Images Using Image Phase Information

SERDAR CAKIR[1], DENIZ CANSEN KAHRAMAN[2], RENGUL CETIN-ATALAY[3], AND A. ENIS CETIN[1,4], (Fellow, IEEE)

[1]Department of Electrical and Electronics Engineering, Bilkent University, Ankara 06800, Turkey
[2]Department of Molecular Biology and Genetics, Bilkent University, Ankara 06800, Turkey
[3]KanSiL Cancer Systems Biology Laboratory, Graduate School of Informatics, Middle East Technical University, Ankara 06800, Turkey
[4]Department of Electrical & Computer Engineering, University of Illinois at Chicago, Chicago, IL 60607 USA

Corresponding author: Rengul Cetin-Atalay (e-mail: rengul@metu.edu.tr).

This work was supported by the Turkish Ministry of Development under KanSiL_2016K121540 Project.

ABSTRACT Contrast enhancement is an important preprocessing step for the analysis of microscopy images. The main aim of contrast enhancement techniques is to increase the visibility of the cell structures and organelles by modifying the spatial characteristics of the image. In this paper, phase information-based contrast enhancement framework is proposed to overcome the limitations of existing image enhancement techniques. Inspired by the groundbreaking design of the phase contrast microscopy (PCM), the proposed image enhancement framework transforms the changes in image phase into the variations of magnitude to enhance the structural details of the image and to improve visibility. In addition, the concept of selective variation (SV) technique is introduced and enhancement parameters are optimized using SV. The experimental studies that were carried out on microscopy images show that the proposed scheme outperforms the baseline enhancement frameworks. The contrast enhanced images produced by the proposed method have comparable cellular texture structure as PCM images.

INDEX TERMS Microscopy images, contrast enhancement, image phase information, Fourier transform, phase contrast microscopy.

I. INTRODUCTION

The process of contrast enhancement has been widely used in various image processing, pattern recognition, and computer vision applications [1]. The main aim of this process is to increase the visibility of objects of interest in order to assist user oriented or automated tasks including object analysis, detection, segmentation, and recognition. In the literature, most of the contrast enhancement techniques are based on modifying the image histogram to improve the contrast [1]. Early global Histogram Equalization (HE) techniques directly modify the histogram without considering the artifacts which may occur on the enhanced image. Moreover, these techniques fail to enhance the local details in the image. Numerous attempts have been made to modify the histogram locally and adaptively in order to eliminate the artifacts on the enhancement results [2]–[6]. Adaptive HE methods [5], [6] divide the image into sub-blocks and perform HE within these sub-blocks. However, when combining the sub-blocks, a ''checker-board'' effect may occur on the boundaries of the blocks due to local contrast changes. In order to eliminate these grid-shaped artifacts, overlapping blocks can be used at the expense of increasing computational complexity and memory. An efficient implementation, called contrast limited adaptive HE (CLAHE) [2], [3], was proposed to overcome the limitations of HE approaches. The CLAHE technique limits the contrast and eliminates the artifacts caused by the mapping of two close gray-scale values to significantly different values. The CLAHE method is usually preferred in offline applications due to its high computational cost. Therefore, there have been several attempts which try to realize the algorithm efficiently for real-time applications [7], [8].

The HE based techniques have been utilized in many medical imaging applications including chest radiography [9], [10], computer tomography (CT) [11], mammography [12], and cell microscopy [13]–[15]. Researchers have widely used HE based approaches as a powerful preprocessing tool for improving visibility and balancing the contrast of cell images [15]–[17].

Phase Contrast Microscopy (PCM) [18] is a well-established optical technique to improve the contrast of the

images of the transparent specimens. The method provides a contrast enhancement for stained biological materials by transforming the phase differences of light, which are caused by differences in refractive index between cellular components, into differences in amplitude of light, i.e., light and dark areas, which can be observed [19]. In this way, PCM enhances the image contrast by converting phase differences into amplitude changes. Based on this fact, we introduce an image enhancement framework inspired by the PCM in order to enhance the visual details in images of transparent specimens. To obtain transformations between phase and amplitude differences in our image enhancement framework, the Discrete Fourier Transform (DFT) of the image is computed and image phase information is extracted. Then the frequency components where the phase transitions are large are amplified with large weights to transform the phase changes into amplitude variations. In addition, a small amount of phase shift is added to the high frequency components. This process eliminates the artifacts on smooth background regions. After the calculation of the inverse DFT, an enhanced image is obtained.

The last step of the overall enhancement process is a modified version of the well-known Total Variation (TV) approach [20]. In denoising and deconvolution applications TV is minimized [20], [21]. In this paper, the TV functional around edges are maximized. Since microscopes have the most expensive optical equipment, there is almost no noise in microscopic images. As a result, edges in the image are enhanced by maximizing the TV within the above constraints. We introduce the concept of Selective Variation (SV) method which maximizes the variations in local regions of interest to achieve sharp transitions around edges. To the best of our knowledge, this is the first paper maximizing the $\ell 1$-norm of a cost functional within a region of interest.

In the literature, most image contrast enhancement methods are in the spatial domain [22]. Also, several attempts have been made to utilize the contrast enhancement process in the frequency domain [23], [24]. The proposed method which is inspired by the PCM, aims to improve the image contrast and enhance the visual details in the image by utilizing a Fourier domain approach.

II. CONTRAST ENHANCEMENT BASED ON FOURIER PHASE INFORMATION

Inspired by the brilliant design of the PCM [18], we propose a contrast enhancement technique by utilizing the image phase information to increase the weight of frequencies where phase variations occur. In general, most natural images are low-pass by nature. In other words, spectral energy is very dense at low frequencies compared to high frequencies in natural images. Sharp transitions and highly structured textures contribute to the high frequency components of an image. In order to emphasize the high frequency components containing important hidden details, it is possible to amplify the high frequency DFT coefficients in Fourier domain. However, frequency-based modifications in Fourier domain should be carried out carefully because improper spectrum manipulations may degrade the natural harmony of the image and cause undesired artifacts in the image domain. Moreover, the modifications must not degrade the conjugate-symmetric nature of the Fourier coefficients.

In the proposed image enhancement algorithm, the high frequency components are emphasized by taking into consideration the image phase. Let $x\,[m, n] \in \mathbb{R}^{M\times N}$ be the $M \times N$ dimensional image. Each computation step of the proposed technique is summarized below:

The algorithm starts by calculating the two dimensional $\hat{M} \times \hat{N}$-point Discrete Fourier Transform (2D-DFT) $X[u, v]$ of the image $x\,[m, n]$. The DFT parameters should be selected as $\hat{M} = 2^p \geqslant M$, $\hat{N} = 2^q \geqslant N$ in order to take advantage of the Fast Fourier Transform (FFT) algorithm where p and q are positive integers. It is important to increase the FFT size by selecting p and q as large as possible for reducing the spectral noise in the enhancement process. Let $X[u, v]$ be:

$$X[u, v] = |X[u, v]|\, e^{j\phi[u,v]} \qquad u = 0, 1, \ldots, \hat{M} - 1 \;\&\; v = 0, 1, \ldots, \hat{N} - 1 \quad (1)$$

Inspired by the PCM framework, a small amount of phase shift (θ) is added to the high frequency components of the image spectrum which are determined by a high-pass mask $H[u, v]$ with cut-off frequency indices u_c and v_c:

$$H\,[u, v] = \begin{cases} 0, & u \leqslant u_C - 1 \;\&\; v \leqslant v_C - 1 \\ 0, & u \leqslant u_C - 1 \;\& \\ & \hat{N} - v_C + 1 \leqslant v \leqslant \hat{N} - 1 \\ 0, & \hat{M} - u_C + 1 \leqslant u \leqslant \hat{M} - 1\& \\ & v \leqslant v_C - 1 \\ 0, & \hat{M} - u_C + 1 \leqslant u \leqslant \hat{M} - 1\& \\ & \hat{N} - v_C + 1 \leqslant v \leqslant \hat{N} - 1 \\ 1, & \text{otherwise} \end{cases} \quad (2)$$

Since low frequency components correspond to the smooth and constant regions of an image, adding phase shift to these components may degrade the quality of the image by resulting in undesired artifacts on smooth regions. However, modifying the phase at high frequencies may reveal the suppressed details in the spectrum. Therefore, the phase shift θ is added only to the high frequencies which are determined by the mask $H[u, v]$, in order to preserve the conjugate-symmetric nature of the spectrum. After the phase shift operation, the spectrum of the image becomes as follows:

$$X_P[u, v] = |X[u, v]|\, e^{j(\phi[u,v] + H(u,v)\theta\, \mathrm{sgn}(\phi[u,v]))} \quad (3)$$

where *sgn* is the sign operator, which is required to preserve the conjugate symmetry property of DFT. In order to emphasize the high frequencies, a weighting scheme is proposed based on the transitions of image phase information between neighboring frequency components. The phase transitions are obtained by computing the phase gradient along horizontal and vertical axes. The phase gradient $\partial_\phi[u, v]$ is computed as

follows:

$$\partial_\phi[u,v] = |\phi[u,v] - \phi[u-1,v]| + |\phi[u,v] - \phi[u,v-1]| \quad (4)$$

After computing the gradient of the image phase, neighboring frequency components which provide significant phase transitions are determined. Let S be the set of spatial locations of the frequency pairs at which the corresponding phase transitions exceed the threshold τ_ϕ:

$$S = \{(u,v) | \partial_\phi[u,v] > \tau_\phi\} \quad (5)$$

The phase transition based weight matrix $W_p(u,v)$ is obtained by using the set S as follows:

$$W_p[u,v] = \begin{cases} \alpha\partial_\phi[u,v], & \text{for } (u,v) \in S \\ 1, & \text{otherwise} \end{cases} \quad (6)$$

where α is a fixed scaling factor. The $W_p[u,v]$ weight matrix may have sharp transitions due to direct thresholding; which may cause undesired artifacts in the reconstruction. To eliminate sharp transitions in the weight matrix $W_p[u,v]$, a 2D-Gaussian function ($g[u,v]$) with parameters μ and σ is utilized to smooth the discontinuities as follows:

$$W_f[u,v] = W_p[u,v] * g[u,v] \quad (7)$$

where "$*$" is the convolution operator. Similar to the phase addition step described in Equation 3, only high frequency components are exposed to weighting in the spectrum by using the high-pass mask $H[u,v]$. As a result, the final weight matrix W is obtained as follows:

$$W[u,v] = \begin{cases} W_f[u,v], & \text{if } H[u,v] = 1 \\ 1, & \text{otherwise} \end{cases} \quad (8)$$

The weight matrix $W[u,v]$ is used to amplify the high frequency components in a clever manner in order to reveal the suppressed details existing at the high frequency components. An example of the final weight matrix $W[u,v]$ is shown in Fig 1.

The weight matrix $W[u,v]$ is applied to the spectrum matrix $X_P[u,v]$ which has been exposed to phase shifts. As a result, the spectrum of the input image is modified in terms of both magnitude and phase after the computation of $X_C[u,v] = W[u,v]X_P[u,v]$.

Inverse DFT (IDFT) of $X_C[u,v]$ is calculated to obtain the contrast-enhanced image. Here, the IDFT is realized using the inverse FFT (IFFT) algorithm:

$$x_C[m,n] = IDFT\{X_C(u,v)\} \quad (9)$$

where $x_C[m,n]$ is the contrast enhanced version of the original image $x[m,n]$.

The level of enhancement of the reconstructed image $x_C[m,n]$ is affected by several parameters including the phase filter cut-off frequency indices u_c, v_c, scaling coefficient α, phase shift θ, phase gradient threshold τ_ϕ, and parameters of the Gaussian smoothing function μ, σ. Therefore, it is important to select the parameters appropriately by maximizing the image contrast. In this study, a Total Variation (TV) based measure is used to maximize the image contrast in a grid search framework. The TV of the original image $x[m,n]$ can be defined as follows [20], [21], [25], [26]:

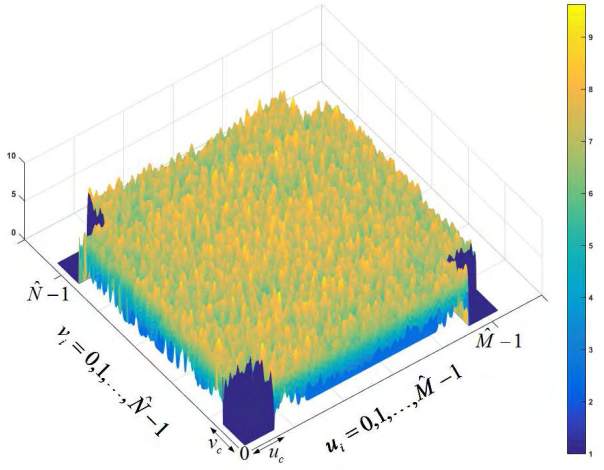

FIGURE 1. $\hat{M} \times \hat{N}$ **sample weight matrix obtained for** $\alpha = 1.5$, $u_c = v_c = 50$, $\tau_\phi = \pi$, $\mu = 13$, $\sigma = 2$, $\hat{M} = 1024$, $\hat{N} = 1024$.

$$\text{TV}(x) = \sum_{m,n} |x[m+1,n] - x[m,n]| + \sum_{m,n} |x[m,n+1] - x[m,n]| \quad (10)$$

Instead of maximizing the TV over the entire image, we select "busy" regions of the image and carry out the optimization process over selected regions. In other words, background pixels are not included in the optimization process. Since only partial image information is used in the calculation of "variation", we define "Selective Variation" (SV) as follows:

$$SV(x_C) = S[m,n] \cdot \left(\sum_{m,n} |x_C[m+1,n] - x_C[m,n]| + \sum_{m,n} |x_C[m,n+1] - x_C[m,n]| \right) \quad (11)$$

where the selected pixels are obtained as follows:

$$S[m,n] = \begin{cases} 1, & x[m,n] > \frac{1}{b^2} \sum_{i=m-\frac{b}{2},}^{m+\frac{b}{2}} \sum_{j=n-\frac{b}{2},}^{n+\frac{b}{2}} x[i,j] + \beta \\ 1, & x[m,n] < \frac{1}{b^2} \sum_{i=m-\frac{b}{2},}^{m+\frac{b}{2}} \sum_{j=n-\frac{b}{2},}^{n+\frac{b}{2}} x[i,j] - \beta \\ 0, & \text{otherwise} \end{cases} \quad (12)$$

where b denotes the overlapping local window size and β is an additive constant which determines a deviation limit for each pixel from the average values of their local blocks. In other

words, the pixels which are greater than β plus the average value of a block, are selected.

The final enhanced image $x_C^*[m,n]$ is obtained by maximizing the SV functional as follows:

$$x_C^*[m,n] = \underset{u_c,v_c,\theta,\tau_\phi,\alpha}{arg\,max} \; SV\,(x_C[m,n])$$
$$\text{subject to } u_c < \frac{\hat{M}}{2}, \quad v_c < \frac{\hat{N}}{2}$$
$$\frac{\pi}{K_1} \leqslant \theta \leqslant \frac{\pi}{K_2},$$
$$c_1\pi \leqslant \tau_\phi \leqslant c_2\pi, \quad \text{and}$$
$$a_1 \leqslant \alpha \leqslant a_2 \tag{13}$$

where K_1, K_2 determines the phase interval added to the high frequency components of the spectrum. The c_1, c_2 coefficients determine the interval of high phase transitions, and a_1, a_2 values are used to limit the scaling coefficient α used in the weighting stage.

The maximization of SV functional is carried out to determine the aforementioned enhancement parameters $u_c, v_c, \theta, \tau_\phi, \alpha$. The maximization process described in Equation 13 is the modified version of the well-known Total Variation (TV) approach [20]. In the literature, most denoising and deconvolution applications are based on TV minimization [20], [21]. In this paper, we use an alternative approach by maximizing the TV functional around edges. Since microscopes use expensive optical equipment, the microscopy images are almost noise-free. As a result, edges in the image are highlighted by maximizing the TV within the constraints described above. The parameter optimization process can be performed only once for a certain family of microscopic images. However, one can repeat the optimization process for any individual image to obtain a custom parameter set for that image.

III. EXPERIMENTAL STUDIES

The performance of the proposed algorithm is compared with the performances of baseline image enhancement methods [3], [23], [24], [27], [28] on two microscopic image sets.

A. IMAGE DATASET

To evaluate the performance of the proposed algorithm, microscopic images of human hepatocellular carcinoma cells (HCC) are captured. HCC cells (Huh7 and Mahlavu) were maintained in Dulbecco's Modified Eagle's Medium (DMEM) (Invitrogen GIBCO), supplemented with 10% fetal bovine serum (FBS) (Invitrogen GIBCO), 2 mM L-glutamine, 0.1 mM nonessential amino acids, 100 units/mL penicillin and 100 g/mL streptomycin at 37 °C in a humidified incubator under 5% CO_2. Before capturing the microscopy images, cells were seeded on 100 mm culture plates and grown until they reached 50-60% confluency. Microscopy images of Mahlavu cells were captured by using Euromex Oxion Inverso OX.2003-PL inverted light microscope (Figure 3 (a) and Figure 5(a)). For Hematoxylin and Eosin staining, Huh7 cells were inoculated onto coverslips in six well plates. Cells were fixed with 100% ice cold methanol once they reached 50-60% confluency. After washing cells with cold 1x PBS, hematoxylin was added onto cells to be incubated for two minutes and washed with tap water. Then, cells were incubated in 1% acid alcohol (1 unit HCl in 100 units of ETOH) for thirty seconds and washing step was repeated. Next, cells were incubated with 1% ammonia solution for thirty seconds and washed. Finally eosin staining was carried out for one minute and washed. Cells were mounted onto slides using glycerol and visualized under Nikon Eclipse 50i upright microscope (Figure 8 (a)) and Nikon Eclipse Ti-S inverted microscope (Figure 8 (b)) using NIS-Elements software. When capturing images using the microscope, two levels of optical zooming were performed. 20x optical zoom provides a wide angle view of the HCC cells. 40x optical zoom enables a narrower field of view and detailed visualization of the organelles of the cells. Totally, 15 images of size 1360 × 1024 were captured using the inverted light microscope.

To increase the number and variability of the dataset, an additional image set is used [29]. This image set contains the microscopy images of native urine sediments. Before capturing the microscopy images, the urine sediments were centrifuged in 2000 rpm and the supernatant was removed and the sediment resuspended to create a tenfold concentrated sample solution [29]. 14 sample microscopy images of native urine sediments were collected from a publicly available report [29] and the images in the document are of size 1213 × 910. Forming an image dataset from microscopy images captured using different imaging devices, environments and purposes enables us to test the proposed algorithm's generalization capability.

The grid search algorithm maximizing Equation 13 stops after covering the whole parameter space defined by the user. At the end, the image providing the maximum SV ($x_C^*[m,n]$) is determined as the output of the proposed enhancement framework. The following parameter space is covered by our scheme:

$$u_c \in \left[1, \frac{\hat{M}}{2}\right], \quad v_c \in \left[1, \frac{\hat{N}}{2}\right], \; \theta \in \left(\frac{\pi}{2^{10}}, \frac{\pi}{2^3}\right),$$
$$\alpha \in (1,3), \quad \tau_\phi \in (0.5\pi, 2.5\pi) \tag{14}$$

The algorithm covers the above parameter space to search for the image that provides the largest SV measure. The proposed framework is implemented in MATLAB environment on a computer containing Intel(R) Core(TM) i5 3.40 GHz processor, 8 GB RAM running on Microsoft Windows 7 operating system. The enhancement of a single image of size 1024×1024 takes approximately 1.68 seconds. Experimental results show that the proposed algorithm obtains satisfactory enhancement results in microscopic images, if the parameters are selected as $u_c = v_c = 15$, $\theta = \pi/32$, $\alpha = 2$, $\tau_\phi = \pi$.

B. OBJECTIVE PERFORMANCE MEASURES

In order to obtain a fair and quantitative performance analysis, objective performance measures are utilized to measure the performance of the algorithms for image enhancement. In this work, ''Color Enhancement Factor (CEF)'' [30], Universal Image Quality Index (UIQI) [31], adaptive edge map (AEM), Histogram Flatness (HF) & Histogram Spread (HS) [32], and Logarithmic Michelson Contrast Measure by Entropy (AMEE) [33] objective measures are used in the performance comparisons.

The first performance measure used in the tests is the CEF measure. The CEF is based on the ratio between the colorfulness measures of the reference and enhanced images. The colorfulness is generally defined as the attribute of chrominance information perceived by a human observer. The image statistics based colorfulness measure was first proposed by Hasler and Süsstrunk [34]. The colorfulness measure is then modified by defining opponent color spaces [30]. Let R, G, and B be the red, green, and blue image channels, respectively. Based on the RGB color space, the opponent color spaces are defined as follows:

$$\alpha = R - G, \quad \beta = \frac{R+G}{2} - B \tag{15}$$

Based on the opponent color spaces, the colorfulness measure C is computed by using the first and second order statistics of α and β as follows:

$$C = \sqrt{\sigma_\alpha^2 + \sigma_\beta^2} + 0.3\sqrt{\mu_\alpha^2 + \mu_\beta^2} \tag{16}$$

where μ_α, μ_β, and σ_α, σ_β are the mean values and standard deviations of the opponent components α and β, respectively. Finally, CEF is obtained by computing the ratio between the colorfulness measures of the reference and the enhanced images as follows:

$$CEF = \frac{C_{enh}}{C_{ref}} \tag{17}$$

The second performance measure used in the experiments is the UIQI [31]. As a full reference image quality measure, the UIQI measure is composed of three main components which evaluate the total quality as the combination of ''loss of correlation'', ''luminance distortion'' and ''contrast distortion'' as follows:

$$UIQI = \frac{\sigma_{xy}}{\sigma_x \sigma_y} \cdot \frac{2\mu_x \mu_y}{\mu_x^2 + \mu_y^2} \cdot \frac{2\sigma_x \sigma_y}{\sigma_x^2 + \sigma_y^2} \tag{18}$$

where μ_x, μ_y, σ_x , and σ_y are the mean values and the standard deviations of the images x and y, respectively. Subsequently, these components are multiplicatively combined in order to generate a final quality score. The UIQI measure takes values in the interval $[-1, 1]$ and higher values of the measure are the indicator of better image enhancement.

The AEM measure is proposed to quantify the efficiency of algorithms in edge preservation on foreground pixels. The AEM measure can be defined as the ratio between the number of foreground edge pixels preserved in the enhanced image and the total number of foreground pixels on the reference image. In order to extract foreground pixels from the reference image, an adaptive local threshold based approach is utilized. The thresholding technique determines a threshold for each pixel by computing the mean around the k-neighborhood of each pixel. In this way, different regions of the image can be thresholded with different values which are calculated by an adaptive approach. Let $I(x, y)$ be the $M \times N$ reference image. The foreground pixels $T(x, y)$ of the reference image are determined as follows:

$$\begin{aligned} T(x,y) &= \begin{cases} 1, & I(x,y) \geqslant \mu(x,y) + \eta \\ 0, & I(x,y) < \mu(x,y) + \eta \end{cases} \\ \mu(x,y) &= \frac{1}{k^2} \sum_{i=x-k}^{x+k} \sum_{j=y-k}^{y+k} I(i,j) \\ x &= 1, \ldots, M \quad y = 1, \ldots, N \end{aligned} \tag{19}$$

where η is an additive constant which determines the minimum level of deviation from the mean to be considered as foreground pixel. In the tests, η is selected as 5. The matrix of foreground pixels $T(x, y)$ is used as a reference to quantify the edge preservation in the enhanced image. The edges of the enhanced image are extracted by using the Sobel operator. Also, in order to eliminate the weak transitions, basic thresholding is utilized. At the end, the binary Sobel edge image $I_{Sobel,bin}(x, y)$ is obtained. The AEM measure, which quantifies the edge preservation rate, is computed as follows:

$$AEM = \frac{\sum_{i=1}^{M} \sum_{j=1}^{N} I_{Sobel,bin}(i,j) \cdot T(i,j)}{\sum_{i=1}^{M} \sum_{j=1}^{N} T(i,j)} \tag{20}$$

By its definition, the AEM measure takes values in the interval $[0, 1]$. Higher values of AEM measure correspond to better preservation accuracies.

Additionally, two objective performance measures based on image histogram [32] are used in the tests. One of the histogram based measures is the HF. HF measure tries to quantify the level of contrast by calculating the ratio between the geometric mean and arithmetic mean of the histogram counts for each histogram bin. Let h_i be the histogram count for the i^{th} histogram bin. Using the h_i's HF is computed as follows:

$$HF = \frac{\left(\prod_{i=1}^{n} h_i\right)^{1/n}}{\frac{1}{n}\sum_{i=1}^{n} h_i} \tag{21}$$

Since the geometric mean of a vector is less than or equal to its arithmetic mean, HF measure takes values between the interval $[0, 1]$.

The other histogram based objective performance measure is HS [32]. The HS measure can be defined as the

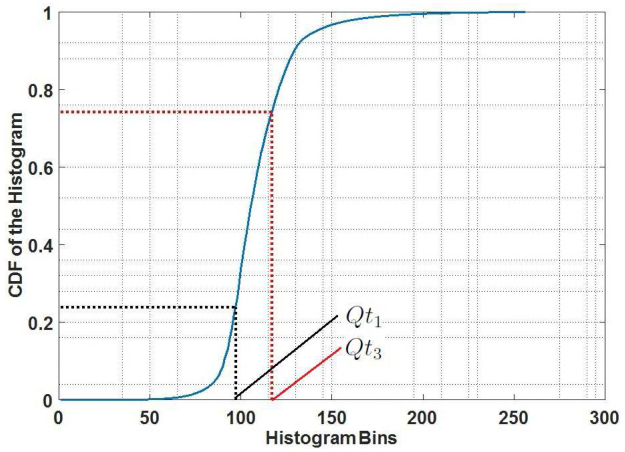

FIGURE 2. Illustration of quartiles Qt_1 and Qt_3.

ratio between the quartile distance and the total range of the histogram. The quartile distance is defined as the difference between the 3^{rd} (Qt_3) and 1^{st} (Qt_1) quartiles. The Qt_1 and Qt_3 correspond to the histogram bins at which the Cumulative Distribution Function (CDF) of the histogram has 25% and 75% of the total histogram counts. The Qt_1 and Qt_3 of an image histogram are illustrated in Figure 2.

By using the 1^{st} and 3^{rd} quartiles, HS measure is evaluated as follows:

$$HS = \frac{Qt_3 - Qt_1}{2^d - 1} \tag{22}$$

where d is the image bit depth. The images used in the tests are 8-bit images ($d = 8$). Since the quartiles lie between the interval $[0, 2^d]$, HS measure takes values between the interval [0, 1].

In the experiments, an additional performance measure, which is based on the ratio between the maximum and minimum values of local image regions, is used. Therefore, the image is divided into non-overlapping sub-blocks. Let $B_{k,l}$ be the (k^{th}, l^{th}) image sub-block. Also, let $I_{max;k,l}$ and $I_{min;k,l}$ be the maximum and minimum intensity values of the sub-block $B_{k,l}$. Using the local maximum and minimum values, the Michelson contrast measure C_M, which is the basis element of the AMEE measure, is defined as follows:

$$C_{M;k,l} = \frac{I_{max;k,l} - I_{min;k,l}}{I_{max;k,l} + I_{min;k,l}} \tag{23}$$

where $C_{M;k,l}$ is the Michelson contrast measure of the k^{th}, l^{th} image sub-block. Using the definition of block-wise Michelson contrast measure $C_{M;k,l}$, the AMEE measures is computed as follows:

$$\begin{aligned} AMEE &= -\frac{1}{RC}\sum_{k=1}^{C}\sum_{l=1}^{R}\alpha\left(C_{M;k,l}\right)^{\alpha}\ln\left(C_{M;k,l}\right) \\ &= -\frac{1}{RC}\sum_{k=1}^{C}\sum_{l=1}^{R}Entropy(C^{\alpha}_{M;k,l}) \end{aligned} \tag{24}$$

Objective performance measures presented in this section provide quantitative evaluations for the enhancement level of the images. However, the enhancement quality of the images are determined by utilizing a "global" approach. With this approach, the enhancement quality is evaluated by a single score for the whole image. In addition to the evaluation of the enhancement performance by a global approach, a more comprehensive performance evaluation methodology is proposed. In this approach, the input image is divided into $N \times N$ non-overlapping sub-blocks. Then, the objective performance measures are calculated for each sub-block. Using the performance scores obtained for each sub-block, the "performance rate plot" of each method is evaluated. The performance rate plots are similar to the success rate plots used in visual object tracking applications [35]. In order to generate performance plots, a performance threshold vector τ_i^P is determined to control the level of enhancement quality. Then, the number of sub-blocks which provide quality scores larger than τ_i^P is counted. This process is repeated for each τ_i^P varying between the range of the corresponding performance measure. At the end, the performance rate is computed as the ratio of sub-blocks which provide quality scores larger than the τ_i^P. The performance rate plots enable a more efficient performance comparison scheme for the contrast enhancement problem. In the experiments, each image is divided into 64×64 sub-blocks. Finally, the performance plots are obtained over 6888 sub-blocks. As an additional performance evaluation criterion, Area Under Curve (AUC) measure is also utilized. The AUC of the performance plot is an indicator to quantify the overall enhancement performance. The AUC measure of each enhancement technique is obtained by computing the area under the performance rate plots.

C. BASELINE ENHANCEMENT ALGORITHMS

In order to test the effectiveness of the proposed phase-based contrast enhancement framework, a comparative performance analysis is carried out by comparing the performance of the proposed technique with the performances of baseline enhancement methodologies. The proposed phase-based contrast enhancement framework is compared with several CLAHE techniques, frequency domain methods, and model based approaches. Three CLAHE frameworks [3], which model the results with different distributions (Rayleigh, uniform, exponential) are used. In addition, a balanced CLAHE approach (BCLAHE) [27], which integrates the process of dynamic range compression and local contrast enhancement, is employed in the comparison. A frequency domain approach based on homomorphic filtering [36] is also used in the comparative analysis. Homomorphic filtering is a well-known technique to enhance images containing illumination variations [36]. A Fourier domain high-pass filtering based approach is also utilized in the comparison. The high-pass (HP) filter used in the tests is the flat version of the weighting scheme presented in Figure 1. The high-pass filter is designed with parameters $u_c = v_c = 15$

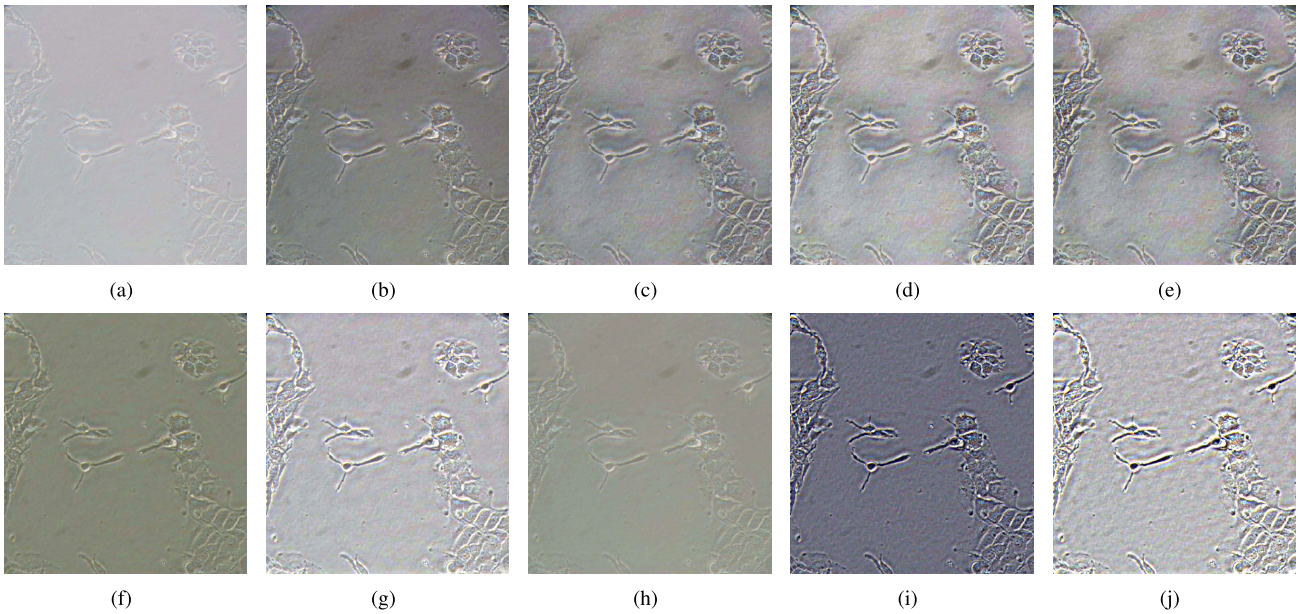

FIGURE 3. The enhancement results of a 40x HHC microscopy image obtained by the proposed and baseline enhancement algorithms. (a) Input image, (b) BCLAHE Image [27], (c) CLAHE Rayleigh [3], (d) CLAHE Uniform [3], (e) CLAHE Exponential [3], (f) Homomorphic Filtering [23], (g) HP Filtering, (h) MEAM [24], (i) Retinex [28], (j) Proposed.

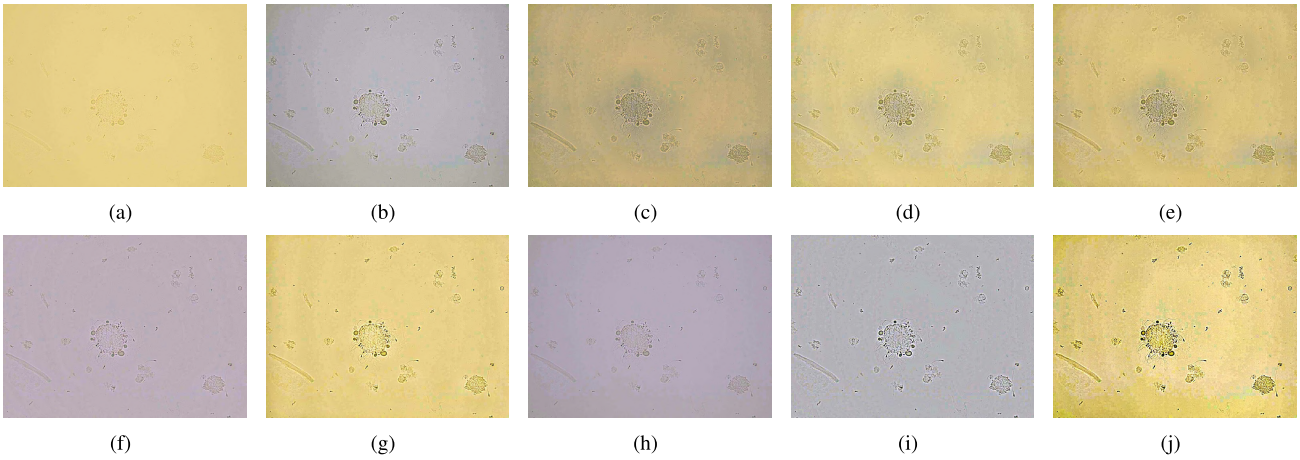

FIGURE 4. The enhancement results of a microscopy image of native urine sediment by the proposed and baseline enhancement algorithms. (a) Input image, (b) BCLAHE Image [27], (c) CLAHE Rayleigh [3], (d) CLAHE Uniform [3], (e) CLAHE Exponential [3], (f) Homomorphic Filtering [23], (g) HP Filtering, (h) MEAM [24], (i) Retinex [28], (j) Proposed.

and $a = 4$ to increase the weight of high frequency components while the low frequency components remain unchanged. Another frequency domain method proposed by Aare Mällo (MEAM) [24] is also studied for comparison purposes. The MEAM method separates an input image into high and low spatial frequency components. By operating separately on the two components, a higher degree of control over the dynamic range compression and contrast enhancement can be realized [24]. The last enhancement method used is the comparison is the Retinex based-enhancement framework [28]. The Retinex is a neuro-physiological model which is defined as the perceived lightness and color by the human vision system. This model is based on the receptive fields which exist in the human visual system. By using a dedicated spatial filter called ''surround'', the lateral opponent operation of the human visual system could be realized [28].

D. EXPERIMENTAL RESULTS

Each image is processed by using the enhancement algorithms described in Section III-C. In the first experiment, the proposed algorithm is compared with the baseline enhancement techniques using 15 microscopy images of human hepatocellular carcinoma cells. The enhancement outputs of the proposed and baseline algorithms for a sample HHC cell image are presented in Figure 3.

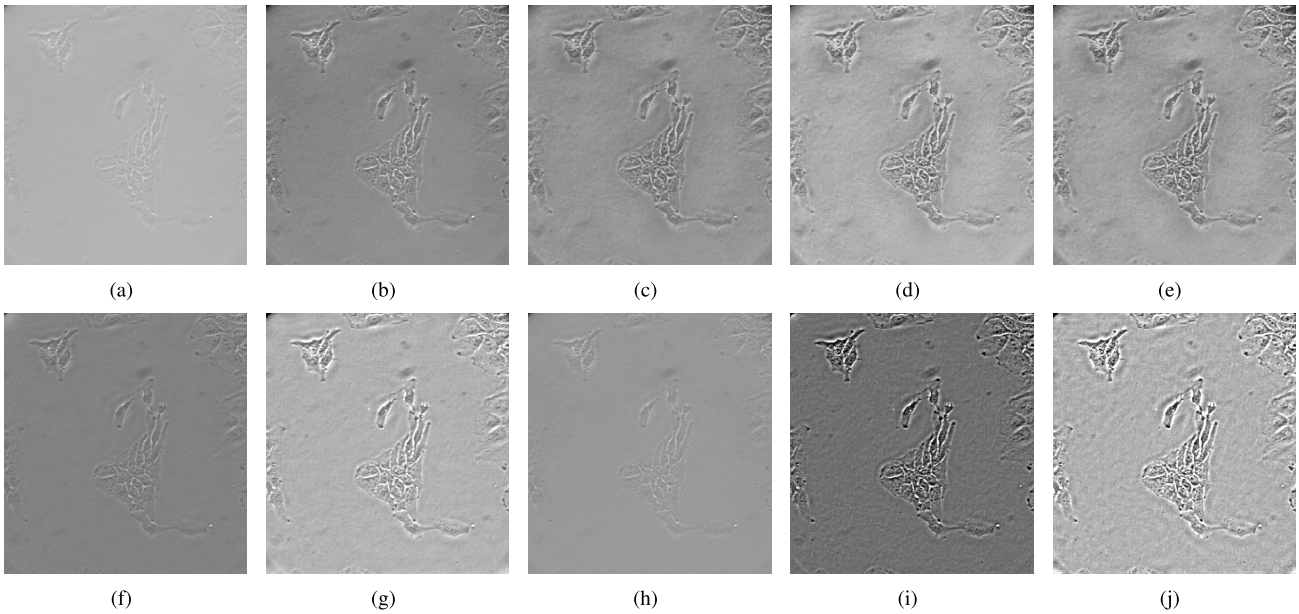

FIGURE 5. The enhancement results of a monochromatic 40x HHC microscopy image obtained by the proposed and baseline enhancement algorithms. (a) Input image, (b) BCLAHE Image [27], (c) CLAHE Rayleigh [3], (d) CLAHE Uniform [3], (e) CLAHE Exponential [3], (f) Homomorphic Filtering [23], (g) HP Filtering, (h) MEAM [24], (i) Retinex [28], (j) Proposed.

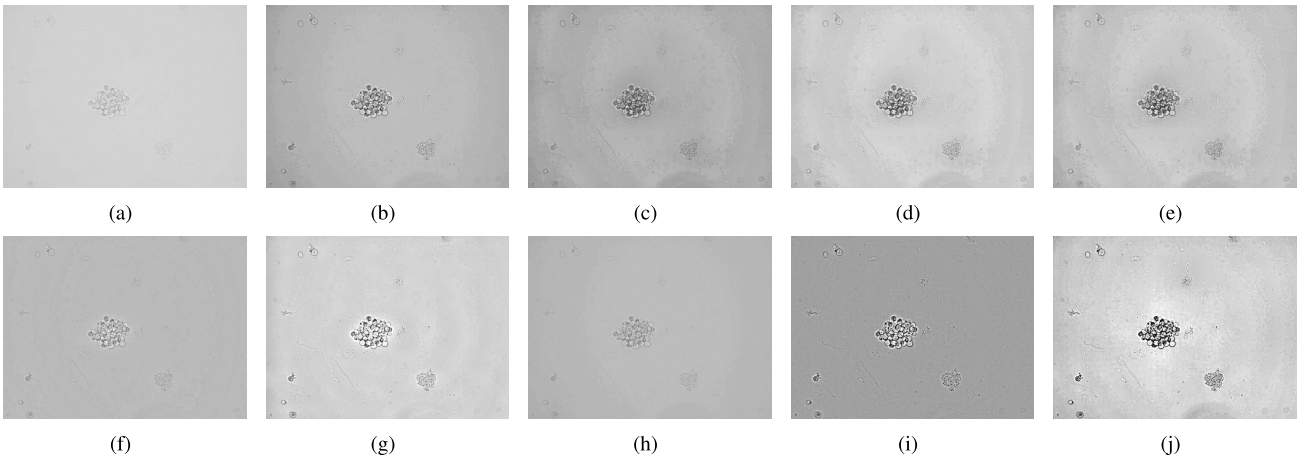

FIGURE 6. The enhancement results of a monochromatic microscopy image of native urine sediment by the proposed and baseline enhancement algorithms. (a) Input image, (b) BCLAHE Image [27], (c) CLAHE Rayleigh [3], (d) CLAHE Uniform [3], (e) CLAHE Exponential [3], (f) Homomorphic Filtering [23], (g) HP Filtering, (h) MEAM [24], (i) Retinex [28], (j) Proposed.

In the second experiment, the proposed and the baseline techniques are utilized for the enhancement of 14 microscopy images of native urine sediments. The enhancement results of a sample microscopy image of native urine sediment are presented in Figure 4.

In the article, monochromatic images are also studied. The performance analysis carried out on color images are repeated for monochromatic images. To obtain monochromatic images, RGB images are converted to the CIE XYZ color space [37]. The luminance component Y of the CIE XYZ space is used for the monochromatic images. The enhancement results for monochromatic microscopy image samples of native urine sediment and HHC cells are presented in Figure 5 and Figure 6.

By examining the enhancement results presented in Figure 3 - Figure 6, CLAHE exponential method, the Retinex algorithm, and the proposed phase-based enhancement framework provide noticeable improvements on image contrast. However, it can be easily observed that the proposed scheme suppresses the background better than the baseline techniques while providing higher contrast. Additionally, the proposed methodology preserves and even enhances the color content of the images. The Retinex approach also provides satisfactory performance on contrast enhancement while suppressing the background efficiently. However, the Retinex algorithm fails to preserve the color information in the enhancement results. Undesired effects on the image such as local shading and darkening can be eliminated more

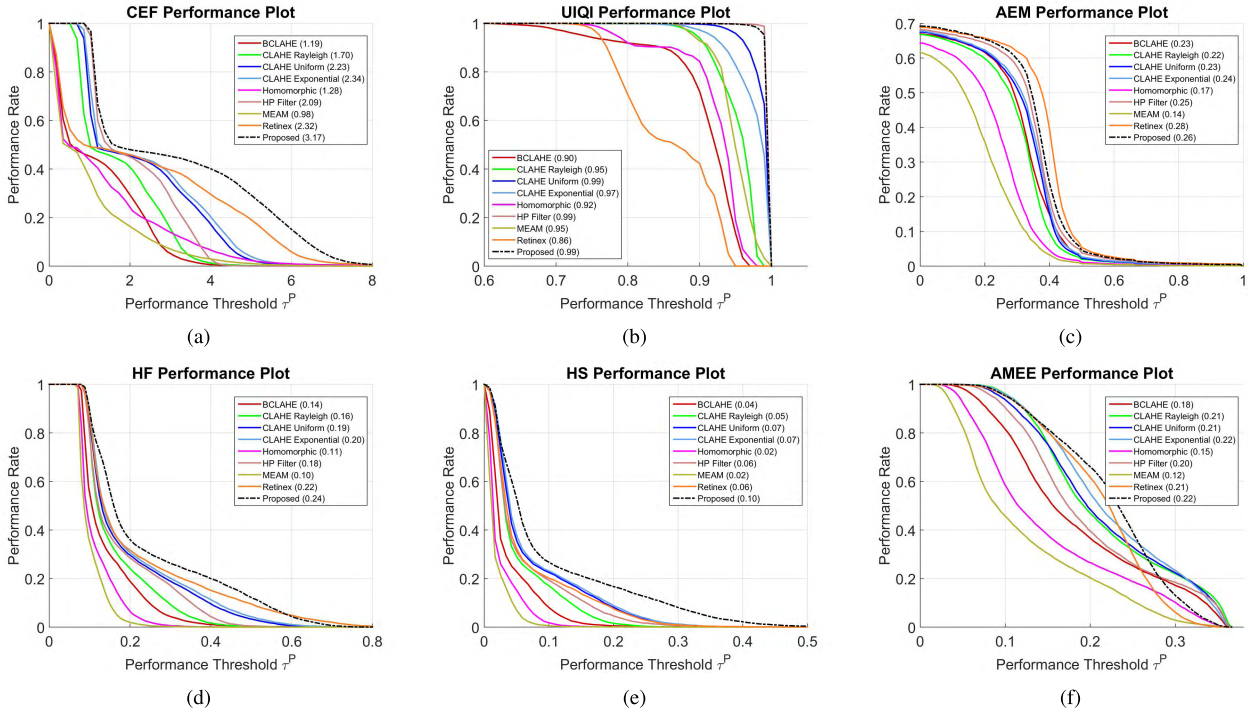

FIGURE 7. **Performance rate plots for objective performance measures. AUC measures for each enhancement framework are presented in the legend of the figure.**

TABLE 1. **Average performance of the enhancement techniques on both RGB and monochromatic images.**

	Objective Performance Measures										
	CEF	UIQI		AEM		HF		HS		AMEE	
	RGB	RGB	CIE-Y	RGB	CIE-Y	RGB	CIE-Y	RGB	CIE-Y	RGB	CIE-Y
BCLAHE [27]	1.295	0.901	0.921	0.360	0.362	0.053	0.049	0.052	0.050	0.185	0.186
CLAHE Rayleigh [3]	1.708	0.950	0.947	0.347	0.336	0.031	0.025	0.055	0.055	0.216	0.206
CLAHE Uniform [3]	2.256	0.987	0.989	0.371	0.360	0.072	0.0583	0.072	0.069	0.217	0.209
CLAHE Exponential [3]	**2.346**	0.974	0.975	0.376	0.366	0.086	0.069	**0.076**	**0.073**	**0.226**	**0.2182**
Homomorphic Filtering [23]	1.181	0.918	0.944	0.298	0.298	0.010	0.009	0.017	0.016	0.150	0.147
HP Filtering	2.163	**0.999**	**0.999**	0.377	0.377	0.059	0.057	0.047	0.043	0.200	0.195
MEAM [24]	0.915	0.948	0.970	0.259	0.260	0.008	0.007	0.025	0.023	0.122	0.122
Retinex [28]	2.321	0.853	0.856	**0.417**	**0.416**	**0.183**	**0.179**	0.045	0.041	0.214	0.212
Proposed	**3.142**	**0.999**	**0.999**	**0.383**	**0.380**	**0.189**	**0.185**	**0.072**	**0.075**	**0.221**	**0.234**

effectively by the proposed scheme. The proposed algorithm also provides more detailed and more significant cell structures which may increase the perceptual awareness of the operator/user.

As discussed in Section III-B, objective performance metrics have been utilized to quantify the enhancement performance. In the objective evaluations, the performance of the proposed scheme is compared with the performances of the baseline techniques using the CEF [30], UIQI [31], AEM, HF&HS [32], and AMEE [33] measures over 29 colored and monochromatic microscopy images. Since the CEF measure quantifies the color enhancement quality, it is not applicable for the tests carried out for monochromatic images. The average performance of each enhancement framework corresponding to each objective measure is presented in Table 1.

In Table 1, the highest two scores obtained for each objective performance measure are written in bold font. By looking at the results presented in Table 1, one can conclude that the proposed technique outperforms the baseline methods in most of the objective quality measures. The Retinex and CLAHE exponential frameworks also provide satisfactory performance on several performance measures. The results presented in Table 1 also show that the enhancement techniques obtain similar results for color and monochromatic images. As stated in Section III-B, the global approach, which is the enhancement evaluation of the whole image with a single score, is not an efficient method to quantify the enhancement quality. Although the results presented in Table 1, which are obtained by the global approach, give an idea about the enhancement performance, a more comprehensive evaluation approach is utilized by constructing performance rate

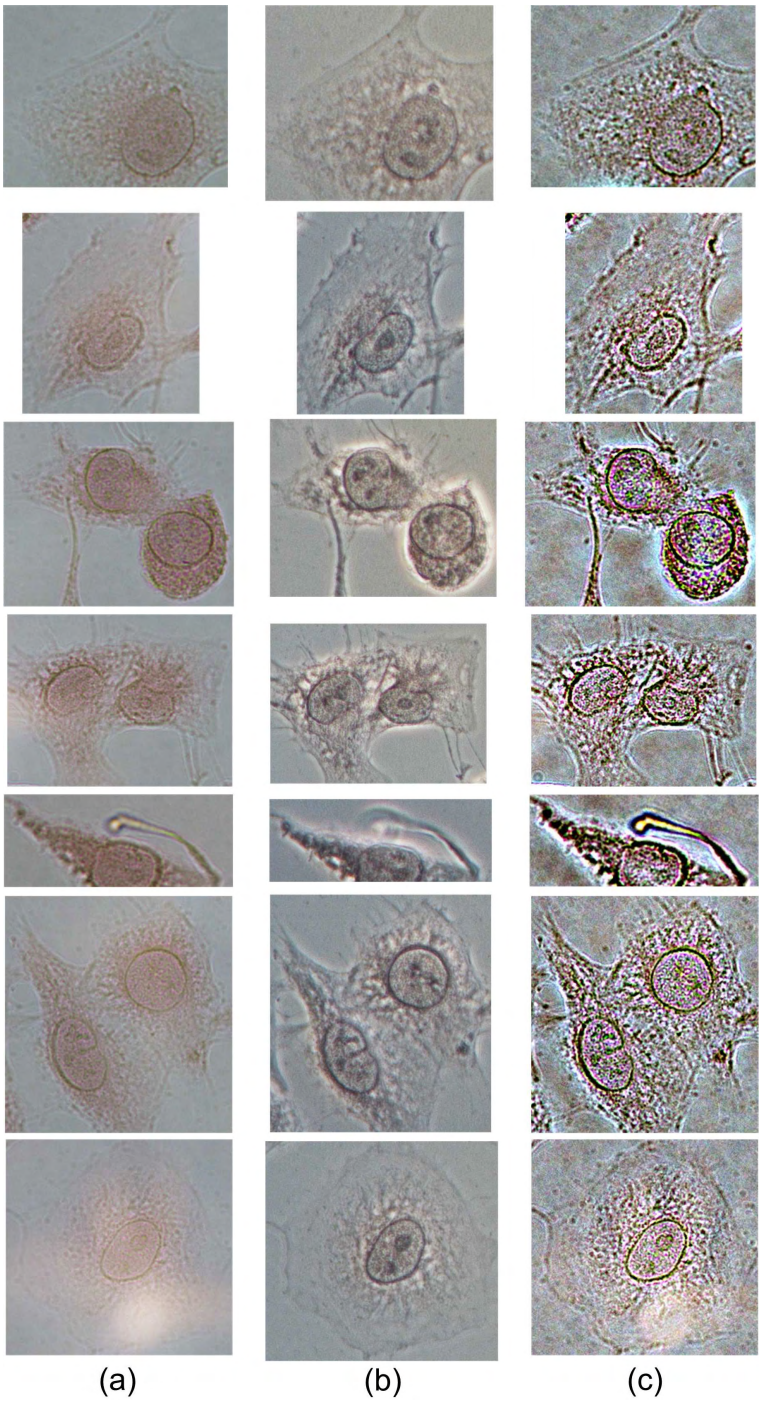

FIGURE 8. The comparison of the proposed technique's outputs with PCM images of hepatocellular carcinoma cells. (a) Images captured by Nikon Eclipse 50i upright microscope (40x). (b) Images obtained by Nikon Eclipse Ti-S inverted PCM microscope (40x). (c) Enhanced versions of the images in (a) using the proposed enhancement framework.

plots for each objective measure. The performance rate plots corresponding to each objective performance measure and enhancement algorithm are presented in Figure 7.

The performance rate plots for the CEF measure (Figure 7(a)) show that the proposed enhancement framework outperforms the baseline techniques on color enhancement. Also, the CLAHE exponential and Retinex methods obtain promising results on color enhancement. Since the AUC measure of the CLAHE exponential technique is slightly higher than the AUC measure of the Retinex framework, the CLAHE

exponential technique can be stated as the contender to the proposed framework for the CEF performance measure. The UIQI performance plots in Figure 7(b) show that the proposed phase-based enhancement technique provides the highest UIQI scores together with the HP filtering technique. The CLAHE uniform method is a strong contender to the proposed algorithm and the HP filtering technique on the UIQI measure. Surprisingly, the Retinex technique which obtains promising results throughout the test, performs poorly on the UIQI measure. This may be caused by the loss of chrominance information in the enhancement results of the Retinex method. The performance rate plots for the AEM measure (Figure 7(c)) show that the Retinex technique provides the best results for the AEM measure. The proposed phase-based scheme obtains comparable results with the Retinex method on the AEM measure. The AEM measure tries to quantify the capability of edge preservation. The Retinex technique and the proposed scheme obtain acceptable level of edge preservation performances in the tests. By looking at the histogram based performance plots (HF&HS) presented in Figure 7(d) and Figure 7(e), one can conclude that the proposed phase-based scheme outperforms the baseline techniques on histogram based performance measures. Although CLAHE based enhancement methods operate directly on the image histogram, the proposed algorithm provides better histogram flatness and histogram spread performances without using any histogram information. The results show the efficiency of the proposed algorithm in balancing the histogram by nature for better enhancement performance. The AMEE performance plots presented in Figure 7(f) show that the proposed enhancement framework achieves the highest performance on entropy-based AMEE measure. The CLAHE exponential and the Retinex techniques obtain comparable results with the proposed framework.

As an additional experiment, the images enhanced by the proposed technique are compared with the PCM images. Therefore, an additional image dataset is gathered by capturing images of hepatocellular carcinoma cells using two different light microscopes. The light microscopy images of cells were captured by Nikon Eclipse 50i upright microscope and Nikon Eclipse Ti-S inverted microscope using NIS-Elements software. The images that were captured by Nikon Eclipse 50i upright microscope are fed in to the proposed enhancement scheme. The images which were captured by Nikon Eclipse Ti-S inverted microscope are used for the comparison of the proposed enhancement scheme's outputs with PCM images.

By examining the images presented in Figure 8, we conclude that the proposed framework provides promising results in contrast enhancement. Most of the cell structures and organelles in the enhanced image become more significant than the ones captured by regular microscopy. Even, the proposed phased based enhancement algorithm introduces some ''halo effects'' near the dark object boundaries. In this way, the proposed method introduces an additional contrast difference between the foreground and background regions which may be useful for visual cell analysis.

IV. CONCLUSION

In this article, an image enhancement framework inspired by the PCM framework is proposed to improve the structural details in microscopy images. The proposed scheme translates phase variations into amplitude changes in order to reveal the suppressed details at high frequency components. In this way, the highly structured regions of cell images become more significant than the background. The performance of the proposed technique is evaluated on two different types of cell microscopy images. Experimental results show that the proposed framework provides satisfactory enhancement performance on color and monochromatic microscopy images of both hepatocellular carcinoma cells and native urine sediments. Moreover, the proposed scheme outperforms the baseline contrast enhancement techniques on objective performance evaluations. The proposed method can be incorporated into microscopic imaging systems of inverted microscopes. The experiment using the H&E stained cells visualized under upright bright field demonstrates that the contrast enhanced images produced by the proposed method have comparable cellular texture structures as PCM images.

REFERENCES

[1] A. K. Jain, *Fundamentals of Digital Image Processing*. Englewood Cliffs, NJ, USA: Prentice-Hall, 1989.

[2] S. M. Pizer *et al.*, ''Adaptive histogram equalization and its variations,'' *Comput. Vis., Graph., Image Process.*, vol. 39, no. 3, pp. 355–368, 1987.

[3] K. Zuiderveld, ''Graphics gems IV,'' in *Contrast Limited Adaptive Histogram Equalization*, P. S. Heckbert, Ed. San Diego, CA, USA: Academic, 1994, pp. 474–485.

[4] Y.-T. Kim, ''Contrast enhancement using brightness preserving bi-histogram equalization,'' *IEEE Trans. Consum. Electron.*, vol. 43, no. 1, pp. 1–8, Feb. 1997.

[5] J.-Y. Kim, L.-S. Kim, and S.-H. Hwang, ''An advanced contrast enhancement using partially overlapped sub-block histogram equalization,'' *IEEE Trans. Circuits Syst. Video Technol.*, vol. 11, no. 4, pp. 475–484, Apr. 2001.

[6] C.-C. Sun, S.-J. Ruan, M.-C. Shie, and T.-W. Pai, ''Dynamic contrast enhancement based on histogram specification,'' *IEEE Trans. Consum. Electron.*, vol. 51, no. 4, pp. 1300–1305, Nov. 2005.

[7] A. M. Reza, ''Realization of the contrast limited adaptive histogram equalization (CLAHE) for real-time image enhancement,'' *J. VLSI signal Process. Syst. Signal, Image Video Technol.*, vol. 38, no. 1, pp. 35–44, 2004.

[8] S. M. Pizer, R. E. Johnston, J. P. Ericksen, B. C. Yankaskas, and K. E. Muller, ''Contrast-limited adaptive histogram equalization: Speed and effectiveness,'' in *Proc. 1st Conf. Vis. Biomed. Comput.*, May 1990, pp. 337–345.

[9] R. H. Sherrier and G. A. Johnson, ''Regionally Adaptive Histogram Equalization of the Chest,'' *IEEE Trans. Med. Imag.*, vol. MI-6, no. 1, pp. 1–7, Mar. 1987.

[10] Y. Li, W. Wang, and D. Yu, ''Application of adaptive histogram equalization to X-ray chest images,'' *Proc. SPIE*, vol. 2321, pp. 513–514, Aug. 1994.

[11] S. M. Pizer, J. D. Austin, J. R. Perry, H. D. Safrit, and J. B. Zimmerman, ''Adaptive histogram equalization for automatic contrast enhancement of medical images,'' *Proc. SPIE*, vol. 0626, pp. 242–250, Jun. 1986.

[12] E. D. Pisano *et al.*, ''Contrast limited adaptive histogram equalization image processing to improve the detection of simulated spiculations in dense mammograms,'' *J. Digit. Imag.*, vol. 11, no. 4, pp. 193–200, 1998.

[13] N. S. P. Kong, H. Ibrahim, C. H. Ooi, and D. C. J. Chieh, ''Enhancement of microscopic images using modified self-adaptive plateau histogram equalization,'' in *Proc. Int. Conf. Comput. Technol. Develop.*, vol. 2. Nov. 2009, pp. 308–310.

[14] Y. Li, Y. Ishitsuka, P. N. Hedde, and G. U. Nienhaus, ''Fast and efficient molecule detection in localization-based super-resolution microscopy by parallel adaptive histogram equalization,'' *ACS Nano*, vol. 7, no. 6, pp. 5207–5214, 2013.

[15] K. Sim, C. Tso, and Y. Tan, "Recursive sub-image histogram equalization applied to gray scale images," *Pattern Recognit. Lett.*, vol. 28, no. 10, pp. 1209–1221, 2007.
[16] P. S. Hiremath, P. Bannigidad, and S. Geeta, "Automated identification and classification of white blood cells (leukocytes) in digital microscopic images," in *Proc. IJCA*, vol. 2. 2010, pp. 59–63.
[17] J. Byun, M. R. Verardo, B. Sumengen, G. P. Lewis, B. S. Manjunath, and S. K. Fisher, "Automated tool for the detection of cell nuclei in digital microscopic images: Application to retinal images," *Molecular Vis.*, vol. 12, pp. 949–960, Aug. 2006.
[18] F. Zernike, "Phase contrast, a new method for the microscopic observation of transparent objects," *Physica*, vol. 9, no. 7, pp. 686–698, 1942.
[19] S. Ruzin, *Plant Microtechnique and Microscopy*. Oxford, U.K.: Oxford Univ. Press, 1999.
[20] L. I. Rudin, S. Osher, and E. Fatemi, "Nonlinear total variation based noise removal algorithms," *Phys. D, Nonlinear Phenomena*, vol. 60, nos. 1–4, pp. 259–268, 1992.
[21] K. Kose, V. Cevher, and A. E. Cetin, "Filtered Variation method for denoising and sparse signal processing," in *Proc. IEEE Int. Conf. Acoust., Speech Signal Process. (ICASSP)*, Mar. 2012, pp. 3329–3332.
[22] C. R. Nithyananda and A. C. Ramachandra, "Survey on histogram equalization method based image enhancement techniques," in *Proc. Int. Conf. Data Mining Adv. Comput. (SAPIENCE)*, Mar. 2016, pp. 150–158.
[23] I. Belykh, "Homomorphic filtering for radiographic image contrast enhancement and artifacts elimination," in *Proc. 3rd Int. Conf. Frontiers Intell. Comput., Theory Appl. (FICTA)*, Cham, Switzerland, 2015, pp. 423–430.
[24] S. Weith-Glushko and C. Salvaggio, "Quantitative analysis of infrared contrast enhancement algorithms," *Proc. SPIE*, vol. 6543, p. 65430S, Apr. 2007.
[25] A. Chambolle, "An algorithm for total variation minimization and applications," *J. Math. Imag. Vis.*, vol. 20, no. 1, pp. 89–97, 2004.
[26] M. Tofighi, O. Yorulmaz, K. Köse, D. C. Yıldırım, R. Çetin-Atalay, and A. E. Çetin, "Phase and TV based convex sets for blind deconvolution of microscopic images," *IEEE J. Sel. Topics Signal Process.*, vol. 10, no. 1, pp. 81–91, Feb. 2016.
[27] F. Branchitta, M. Diani, G. Corsini, and A. Porta, "Dynamic-range compression and contrast enhancement in infrared imaging systems," *Opt. Eng.*, vol. 47, no. 7, p. 076401, 2008.
[28] Z.-U. Rahman, D. J. Jobson, and G. A. Woodell, "Retinex processing for automatic image enhancement," *J. Electron. Imag.*, vol. 13, no. 1, pp. 100–110, 2004.
[29] M. Benovska, J. Tumova, and O. Wiewiorka. (2016). Microscopic Analysis of Urine [Online]. Faculty Med., Masaryk Univ., Brno, Czech Republic. [Online]. Available: https://is.muni.cz/do/rect/el/estud/lf/js15/mikroskop/web/index_en.html
[30] Y.-Y. Fu, *Color Image Quality Measures and Retrieval*. Newark, NJ, USA: New Jersey Inst. Technol., 2006.
[31] Z. Wang and A. C. Bovik, "A universal image quality index," *IEEE Signal Process. Lett.*, vol. 9, no. 3, pp. 81–84, Mar. 2002.
[32] A. K. Tripathi, S. Mukhopadhyay, and A. K. Dhara, "Performance metrics for image contrast," in *Proc. Int. Conf. Image Inf. Process.*, Nov. 2011, pp. 1–4.
[33] S. Gupta and R. Porwal, "Appropriate contrast enhancement measures for brain and breast cancer images," *Int. J. Biomed. Imag.*, vol. 2016, Mar. 2016, Art. no. 4710842.
[34] D. Hasler and S. Süsstrunk, "Measuring colourfulness in natural images," *Proc. SPIE*, vol. 5007, pp. 87–95, Jan. 2003.
[35] Y. Wu, J. Lim, and M.-H. Yang, "Online object tracking: A benchmark," in *Proc. IEEE Conf. Comput. Vis. Pattern Recognit.*, Jun. 2013, pp. 2411–2418.
[36] T. K. Agarwal, M. Tiwari, and S. S. Lamba, "Modified histogram based contrast enhancement using homomorphic filtering for medical images," in *Proc. IEEE Int. Adv. Comput. Conf. (IACC)*, Feb. 2014, pp. 964–968.
[37] M. Tkalcic and J. F. Tasic, "Colour spaces: Perceptual, historical and applicational background," in *Proc. IEEE Region (EUROCON)*, vol. 1. Sep. 2003, pp. 304–308.

SERDAR CAKIR received the B.S. degree in electrical and electronics engineering from Osmangazi University in 2008 and the M.S. and Ph.D. degrees in electrical and electronics engineering from Bilkent University, Ankara, Turkey, in 2010 and 2018, respectively. In 2010, he joined TUBITAK BILGEM ILTAREN, where he is currently a Senior Research Scientist. His main research interests are image/video processing, computer vision, pattern recognition, and infrared imagery.

DENIZ CANSEN KAHRAMAN received the B.Sc. and Ph.D. degrees in molecular biology and genetics from Bilkent University, Ankara, Turkey, in 2011 and 2018, respectively. Her research interests include discovery of novel small molecule kinase inhibitors against liver cancer and cancer stem cells.

RENGUL CETIN-ATALAY received the Ph.D. degree from the Universit de Paris-Sud, Orsay, France, in 1997. She was a French Government Scholar, during her Ph.D. She carried out her doctoral studies as a Research Assistant at Ecole Polytechnique, Paris, France. From 1997 to 2014, she was a Faculty Member at Bilkent University. She was an Assistant Professor at the Virginia Bioinformatics Institute, Virginia Polytechnic Institute and State University, Virginia, USA, during her sabbatical leave in 2004. She is currently a Faculty Member with Middle East Technical University, Ankara, Turkey. Her research interests lie in the fields of bioinformatics and molecular cellular biology of liver cancer.

A. ENIS CETIN (F'10) studied electrical engineering at the Middle East Technical University. He received the B.Sc., M.S.E., and Ph.D. degrees in systems engineering from the Moore School of Electrical Engineering, University of Pennsylvania, Philadelphia. From 1987 to 1989, he was an Assistant Professor of electrical engineering at the University of Toronto, Canada. In 1988, 1991, 1992, he was with Bell Communications Research (Bellcore), NJ, USA. From 1996 to 1997, he was at the University of Minnesota, Minneapolis, USA, as a Visiting Associate Professor. Since 1989, he has been with Bilkent University, Ankara, Turkey, where he is currently a Full Professor. His research interests include signal and image processing, human-computer interaction using vision and speech and audiovisual multimedia databases. He was an Associate Editor of the IEEE TRANSACTIONS ON IMAGE PROCESSING from 1999 and 2003, and a Member of the SPTM Technical Committee of the IEEE Signal Processing Society. He is currently the Editor-in-Chief of the *Signal, Image, and Video Processing Journal*.